

Osteoblast adhesion and matrix mineralization on sol–gel-derived titanium oxide

Maria C. Advincula^a, Firoz G. Rahemtulla^{a,b}, Rigoberto C. Advincula^{c,d}, Earl T. Ada^e, Jack E. Lemons^{a,b,1}, Susan L. Bellis^{a,f,*}

^aDepartment of Biomedical Engineering, University of Alabama at Birmingham, Birmingham, AL 35294, USA

^bThe School of Dentistry, University of Alabama at Birmingham, Birmingham, AL 35294, USA

^cDepartment of Chemistry, University of Alabama at Birmingham, Birmingham, AL 35294, USA

^dDepartment of Chemistry, University of Houston, Houston, TX 77204, USA

^eCentral Analytical Facility, School of Mines and Energy Development, University of Alabama, Tuscaloosa, AL 35487-0164, USA

^fDepartment of Physiology and Biophysics, University of Alabama at Birmingham, 982A MCLM, 1918 University Boulevard, Birmingham, AL 35294, USA

Received 20 May 2005; accepted 6 November 2005

Available online 28 November 2005

Abstract

The biological events occurring at the bone–implant interface are influenced by the topography, chemistry and wettability of the implant surface. The surface properties of titanium alloy prepared by either surface sol–gel processing (SSP), or by passivation with nitric acid, were investigated systematically using X-ray photoelectron spectroscopy, scanning electron microscopy, atomic force microscopy and contact angle metrology. The bioreactivity of the substrates was assessed by evaluating MC3T3-E1 osteoblastic cell adhesion, as well as by in vitro formation of mineralized matrix. Surface analysis of sol–gel-derived oxide on Ti6Al4V substrates showed a predominantly titanium dioxide (TiO₂) composition with abundant hydroxyl groups. The surface was highly wettable, rougher and more porous compared to that of the passivated substrate. Significantly more cells adhered to the sol–gel-coated surface, as compared with passivated surfaces, at 1 and 24 h following cell seeding, and a markedly greater number of mineralized nodules were observed on sol–gel coatings. Collectively our results show that the surface properties of titanium alloy can be modified by SSP to enhance the bioreactivity of this biomaterial.

© 2005 Elsevier Ltd. All rights reserved.

Keywords: Sol–gel technique; Titanium oxide; Surface topography; Wettability; Osteoblast

1. Introduction

The healing of tissues after surgical placement of biomaterials is associated with numerous cellular and extracellular events including the adsorption of proteins at the implant surface [1,2]. Some of the proteins within blood, for example, fibronectin and vitronectin, are known ligands for the integrin family of cell adhesion receptors, and

accordingly, the adsorption of these proteins to biomaterials can promote the adhesion of multiple cell types, including bone-derived cells [3–6]. Integrin-mediated cell adhesion is associated with signaling events and alterations in gene transcription that ultimately regulate cell behaviors such as osteoblast-mediated mineralization of an extracellular matrix [4–6]. Substantial evidence suggests that cell attachment, and the cytoskeletal rearrangement that follows “cell spreading”, are highly dependent on the nature and conformation of adsorbed proteins, and these features of protein adsorption are regulated, in turn, by both the specific surface properties of the biomaterial and the affinity of proteins for the substrata [7,8].

Biological tissues typically interact with the outermost atomic layers of an implant [9], and therefore the surface

*Corresponding author. Department of Physiology and Biophysics, University of Alabama at Birmingham, 982A MCLM, 1918 University Boulevard, Birmingham, AL 35294, USA. Fax: +1 205 975 9028.

E-mail addresses: jlemons@uab.edu (J.E. Lemons), bellis@physiology.uab.edu (S.L. Bellis).

¹Also correspondence to: 615 SDB, 1530 3rd Ave S, Birmingham, AL 35294, USA. Fax: +1 205 975 6108.

oxide properties of the implant play an important role in the initial host response. Titanium and its alloys show excellent biocompatibility, good implant fixation due to the surface reactive oxide, and a high degree of mechanical strength and corrosion resistance [10]. Surface composition, topography and wettability are among the properties known to regulate a number of biological events including protein adsorption, cell attachment, and other aspects of cell behavior including proliferation and differentiation [11–20].

Surface treatment modalities such as anodic oxidation, thermal vacuum deposition, chemical vapor deposition, sputtering, sol–gel process and passivation are commonly employed to modify surface composition and thickness [21–24]. Simple chemical treatments such as immersion in HNO_3 , H_2O_2 , or reducing acids like H_2SO_4 , HCl or H_3PO_4 , alter the surface charge density or microstructure of the surface to produce a more bioactive TiO_2 layer [24–27]. The sol–gel technique is a wet chemical process used to produce metallic oxide glass, bioceramic and bioactive titania-like surfaces [28–30]. Sol–gel coatings have demonstrated good bioactivity due to abundant hydroxyl (OH) groups on the surface that promote nucleation of calcium apatite or formation of mineralized matrix by osteoblasts [31–34]. Thin film oxide coatings can also be prepared by a stepwise surface sol–gel process (SSP) [35]. SSP refers to the sol–gel reaction proceeding only on the surface of a substrate to form a monolayer of thin TiO_2 one cycle at a time, in contrast to the bulk sol–gel technique. The process proceeds in a stepwise manner of chemisorption of an OH-functionalized surface in a metal alkoxide solution followed by rinsing, hydrolysis and drying of the film. A calcination process may be applied if a denser, more crystalline, oxide is desired [35,36]. The process is readily applied to any hydroxylated surface using a metal alkoxide reactive to OH groups, and the sol–gel procedure is independent of each cycle, which allows individual layers to be nanostructured [37,38]. The nanoscale thickness of titanium oxide produced by SSP may be useful in the fabrication of photonic devices, sensors, multicomponent organic films or composite coatings, and molecular templates where the physico-chemical and electrical properties of the film depend on being able to control the nanostructure [36,39–42]. There is a paucity of fundamental information, however, regarding the use of SSP as a modification technique for common metallic biomaterials such as titanium and its alloys. In addition, the effect of this modification on biological systems needs to be further investigated. There are many theoretical advantages in modifying biomaterial surfaces with the stepwise SSP including: modification of the oxide properties to investigate the relative influence of various physico-chemical features such as surface topography, composition, wettability and thickness; nanostructured multilayer organization of the oxide with biologically relevant molecules; and enhanced bioreactivity of the material.

In the current investigation, the preparation of surface sol–gel processed titanium oxide on titanium alloy (Ti6Al4V), and the systematic analysis of the surface topography, chemical composition and wettability of the thin film, are described. The effects of these properties on the initial attachment of osteoblast-like MC3T3-E1 cells, and the in vitro formation of a mineralized matrix (collectively referred to as “bioreactivity” in this paper), were also investigated. The findings are compared with results from commonly passivated titanium alloy.

2. Materials and methods

2.1. Surface activation

Titanium alloy (Ti6Al4V) disks (diameter of 1.27 cm, thickness of 0.64 cm) were mechanically polished using Si carbide papers starting from grade 240, 320, 400 to 600 grits. The samples were sonicated sequentially in acetone, ethanol and water for 10 min each to degrease and clean the surface, followed by immersion in 30/70 v/v % solution of H_2O_2 and H_2SO_4 (Fisher Scientific, Inc., Pittsburgh, PA) for 10 min. This solution, also known as *Piranha* acid solution, removes the native oxide and forms a fresh OH-rich oxide on the surface [43]. Following treatment with *Piranha* solution, the substrates were sonicated three times in ultrapure deionized (DI) water (resistivity = 8.2 M Ω , pH = 6.82, Millipore Inc.), then three times in methanol, before drying with N_2 gas (samples prepared in this manner are hereafter referred to as “acid-etched”). Another set of polished Ti6Al4V disks was cleaned and passivated with 30% HNO_3 for 1 h per ASTM F86 protocol. This set was denoted as “passivated” Ti6Al4V.

2.2. Coating

Acid-etched samples (as described above) were coated with titanium oxide on the surface using the surface sol–gel technique [35]. Briefly, the disks were immersed in 100 mm solution of titanium butoxide (Aldrich) in 1:1 toluene (Sigma, St. Louis, MO) and ethanol (Sigma) for 5 min in a sealed screw cap jar after being purged with N_2 gas. The titanium butoxide reacted with the OH-functionalized surface of titanium during this chemisorption process. After rinsing with copious amounts of solvent to remove unbound alkoxides, the samples were immersed in DI water for 1 min to hydrolyze the alkoxide and regenerate the OH groups on the newly formed titanium oxide coating. The coated disks were then dried by purging with N_2 gas. Chemisorption, rinsing, hydrolysis, and drying were repeated for 5 or 15 cycles. The samples were then stored in a desiccator prior to analysis. This set of coated substrates was denoted as “sol–gel-coated” Ti6Al4V. A schematic diagram is shown in Fig. 1.

2.3. Surface characterization

2.3.1. Compositional analysis

X-ray photoelectron spectroscopy (XPS) analysis was performed in a Kratos Axis 165 electron spectrometer using a 165 mm mean radius concentric hemispherical analyzer operated in fixed analyzer transmission mode at pass energies of 160 eV for survey scans and 80 eV for high-resolution scans. Two to four samples from each type of treatment were analyzed, and highly reproducible results were obtained. A non-monochromatic $\text{AlK}\alpha$ X-ray source (1486.6 eV) was used to excite the photoelectron spectrum. Typical sampling depth of the analysis was about 3 nm from the surface [44]. The analyzed area was approx. 0.8 mm \times 0.2 mm and the chamber pressure during XPS analysis was $<1 \times 10^{-9}$ Torr. Low-energy electrons emanating from an integral charge neutralizer system in Axis 165 compensated the sample surface charge build-up during XPS analysis. The binding energy scale was referenced to the adventitious carbon C1 s at 285.0 eV. A sputter depth profile analysis

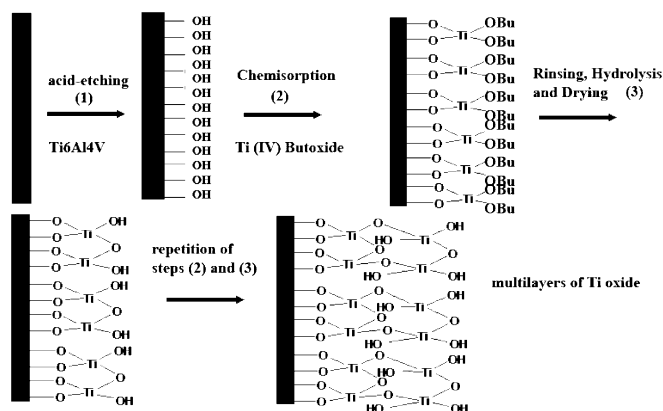


Fig. 1. Schematic diagram of the surface sol-gel process on Ti6Al4V substrates with the subsequent steps of (1) hydroxylation of the substrate using Piranha acid, (2) immersion of the substrate in a solution of titanium (Ti) butoxide in 1:1 toluene:ethanol and (3) rinsing the substrate, immersion in water and drying. Repetition of chemisorption, rinsing, hydrolysis and drying produces multilayers of the oxide.

of the oxide was done using a 4 keV Ar⁺ ion gun with an etch rate of 5 nm/min previously determined for the instrument using a standard 100-nm-thick silicon dioxide sample. Chemical state information was obtained by performing peak fit analysis of the Ti2p and O1s photoelectron lines after a Shirley background correction and by using pure Gaussian lineshapes as models for the component peaks of each peak envelope. Surface atomic composition data were obtained using the sensitivity factors included in the Vision data processing software of Axis 165.

2.3.2. Wettability

Wettability and surface energy of the substrates were determined by the half angle method using a contact angle meter, model CAM-MICRO (Tantec Inc., Schaumburg, IL). Polar (water) and non-polar (methylene iodide) liquids were used to determine the polar and dispersive components, respectively. These values were calculated using the formula integrated in the surface energy software kit of CAM-MICRO. Three samples per group were analyzed, with at least 1–3 spots per disk tested. Three independent experiments were conducted.

2.3.3. Morphology and roughness

A Philips XL30 SEM was used to obtain secondary electron images at primary beam energies of 10–15 keV. Elemental composition was obtained by X-ray fluorescence analysis using the Energy-Dispersive Spectrometer (EDS) attachment of the SEM. The typical sampling depth was a few microns [45]. Atomic force microscopy (AFM) images of sol-gel-coated disks were obtained using a PicoScan system (Molecular Imaging, Phoenix, AZ) equipped with a 7 × 7 μm scanner. All images were collected at magnetic alternating current (MAC[®]) mode in air. The AFM tip consisted of a MAC lever[®] silicon-nitride-based cantilever coated with magnetic film. The force constant of the tip was around 0.5 N/m and the resonance frequency was around 100 kHz. The average roughness represented by the root mean square (rms) roughness of the surface (which is the standard deviation of the mean Z values) was calculated based on a standard formula integrated in the software. The sampling areas were 3 μm × 3 μm and 7 μm × 7 μm. The rms values of five spots per disk were measured and averaged.

2.4. Cell culture

MC3T3-E1 osteoblast-like cells were cultured in alpha-Minimal Essential Medium (αMEM), 10% fetal bovine serum (FBS), 200 mg/ml L-glutamine, and penicillin-streptomycin sulfate (100 U ml⁻¹/100 μg/ml⁻¹), fed every 2–3 days until confluency and split at a ratio of 1:2.

Passages 8–11 were routinely used. To re-seed cells onto the biomaterials disks, the cells were detached from tissue culture flasks by incubating with pronase (Sigma) at 37 °C and the reaction stopped with complete protease inhibitor cocktail tablets (Roche Diagnostics, Indianapolis, IN). Cell viability was assessed by the trypan blue exclusion test prior to cell adhesion assays. All of the material substrates used for cell biological assays were sterilized by immersion in 70% ethyl alcohol for 30 min, followed by exposure to UV light for 24 h.

2.5. Adhesion assay

Cells were plated on 5-layer sol-gel-coated and passivated disks at a density of 1 × 10⁵ cells ml⁻¹ at 37 °C in 24-well tissue culture plates, and were then incubated for 1 or 24 h in serum containing media. After incubation, the disks were washed with phosphate-buffered saline solution (PBS) three times to remove non-adherent cells and the disks were then transferred to new wells. Adherent cells were quantified using the hexosaminidase assay [46]. Three independent experiments were performed, with each experiment performed in triplicate.

2.6. Morphology

Cells adherent to the disks for 1 or 24 h were fixed by incubation in 3.7% formaldehyde dissolved in PBS for 10 min. at room temperature. The disks were then washed two times with PBS and treated with 1% Triton X-100 in PBS for 5 min to permeabilize the cells. After rinsing gently with PBS, the disks were blocked for 10 min with 1% heat-denatured bovine serum albumin (“dBSA”, prepared by heating at 80 °C for 5 min), and the actin cytoskeleton was subsequently labeled by incubation in rhodamine-phalloidin (Molecular Probes, Inc, Eugene, Oregon) for 40 min at 37 °C. Counterstaining of nuclei was done with Hoechst stain (Sigma). The disks were rinsed in PBS, then mounted on glass slides using Fluoromount (Southern Biotechnology Associates Inc, Birmingham, AL). The cells were visualized with a Leica Orthoplan fluorescent microscope.

2.7. Mineralization

Cells were seeded onto the biomaterials, and then grown in mineralization media for 14 days. The mineralization media consisted of the culture media previously described, supplemented with 2 mM β-glycerophosphate (Sigma) and 25 μg/ml ascorbic acid (Sigma). Calcein staining of the cultures was performed at day 14 using a modified protocol [47]. Briefly, the cells were incubated with calcein (ICN Biomedicals Inc, Aurora, OH) at 5 μg/mL in mineralizing media for 24 h at 37 °C, after which the disks were washed 3 × in PBS with agitation, and then fixed with 3.7% formaldehyde/PBS for 10 min. The disks were washed two times with PBS, then treated with 1% Triton X-100 in PBS for 5 min. After rinsing gently with PBS, the disks were treated with 1% dBSA for 10 min. After rinsing three times with PBS, the stained disks were mounted on glass slides using Fluoromount and visualized with the fluorescent microscope.

2.8. Statistical analysis

Statistical analysis was performed using SPSS software. Data sets were tested for normality by the Shapiro–Wilk test for normality. Independent sample *t*-test was used to analyze samples within normal distributions and non-parametric *t*-test (Mann–Whitney test) on non-normal samples. The null hypotheses addressed in this paper were: (1) sol-gel coating alters the topography, roughness, composition and wettability of titanium alloy; and (2) sol-gel-coated titanium alloy promotes better cell attachment and mineral formation in vitro than passivated titanium alloy, due to the altered bioactive surface properties.

3. Results

3.1. Composition

Representative wide-scan XPS spectra of the passivated and 5-layer sol-gel-coated Ti6Al4V substrates are shown in Fig. 2 and their corresponding surface atomic composition is given in Table 1. The acid-etched sample is also shown to separate the effect of hydroxylation on the surface composition. The major surface constituents found for the three samples are O, Ti, and C. The ratio of the total O to Ti atoms for the passivated sample (2.8) was found to be significantly lower than that of sol-gel-coated samples (6.8).

The data in Fig. 3 shows the O1s spectra fitted into three component peaks, as previously reported in the literature [48]. The component peak at 530.3 eV is assigned to the lattice oxide while the high binding energy components at 532.0 and 533.2 eV are assigned to OH and adsorbed H₂O, respectively. The OH percentage compositions on the surface after HNO₃ passivation and sol-gel deposition were approximately 19.5% and 34.6%, respectively. The results in Fig. 3 likewise indicate a much higher relative amount of adsorbed H₂O on the sol-gel-coated surface (28.9% H₂O) than on the passivated surface (H₂O not detected).

The data in Fig. 4 illustrate the typical evolution of the Ti2p peak lineshape at various selected stages of the sputter

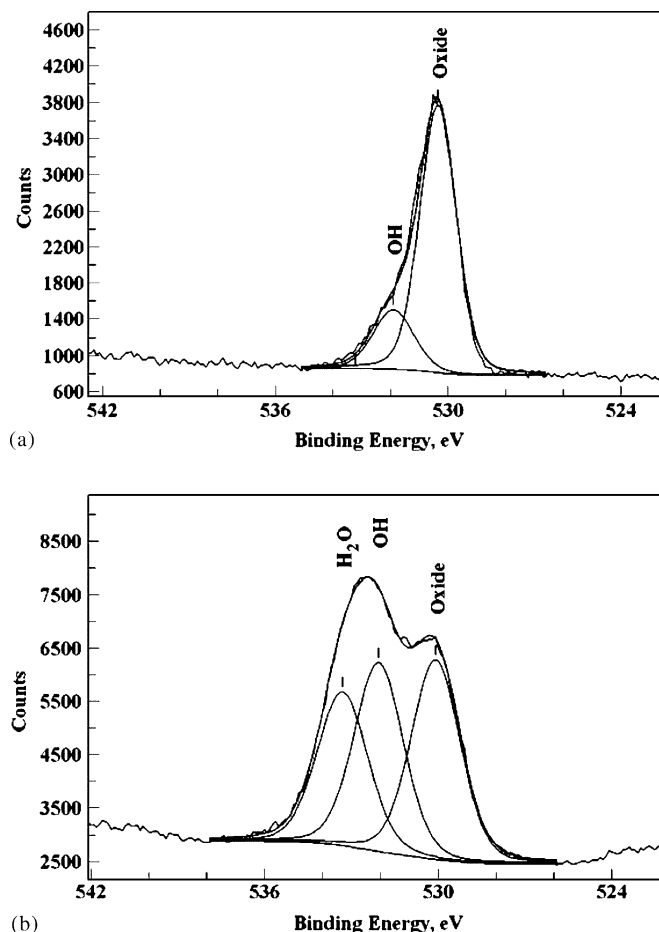


Fig. 3. High-resolution scan of O1s spectra showing the component peaks: (a) passivated, and (b) 5-layer sol-gel-coated Ti6Al4V.

depth profile analysis for the sol-gel-coated sample. Similar lineshape analysis plots for the passivated samples were made, but are not shown here. The sputter depth profile plots in Fig. 5 display the Ti chemical states as a percentage of the total Ti for the passivated and the 5-layer sol-gel-coated Ti6Al4V substrates. Approximately 16% substoichiometric Ti_xO_y oxide states were detected on the surface of the passivated sample, while the sol-gel-coated sample appears to have a significantly higher proportion of the Ti_xO_y states within the oxide film. Moreover, for the passivated sample, about 12% of the total surface Ti signal was found to be from elemental Ti⁰ contribution. In contrast, only fully oxidized TiO₂ states were found on the surface of the sol-gel-coated sample.

3.2. Wettability and surface energy

The surface wettability and surface energy were determined by measuring the contact angles of polar (water) and non-polar (methylene iodide) liquids on the passivated and 5-layer sol-gel-coated surfaces. The total surface energy is the sum of the polar and dispersive components. The surface energy calculation was based on the geometric

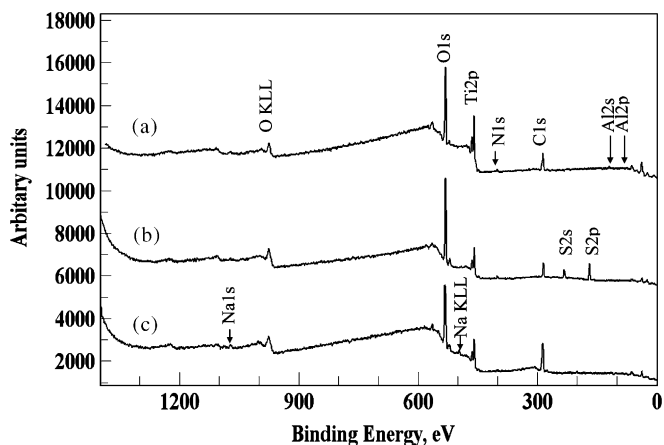


Fig. 2. Representative wide-scan XPS spectra of (a) passivated Ti6Al4V, (b) acid-etched (prior to sol-gel coating) and (c) 5-layer sol-gel-coated Ti6Al4V.

Table 1
Atomic percentage composition of the different substrates

	% O	% Ti	% C	% Al	% N	% S	% Na
Passivated	45.9	16.6	30.9	4.7	1.8	nd ^a	nd
Acid etched	49.9	6.1	30.0	1.4	3.4	9.2	nd
Sol-gel	43.5	6.4	48.0	nd	1.4	nd	0.8

^and = not detected.

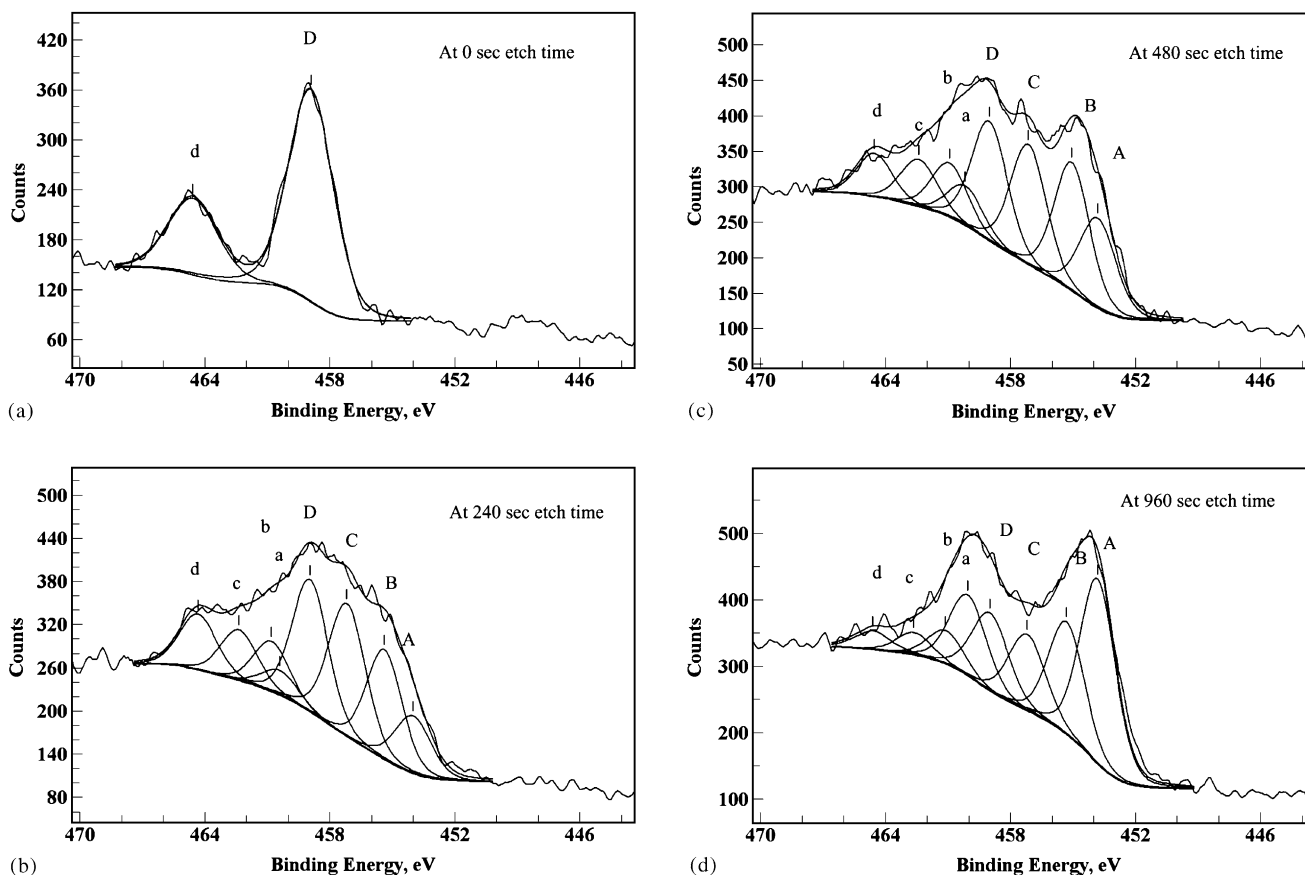


Fig. 4. Typical evolution of the Ti2p spectral peak envelope during sputter depth profiling for the 5-layer sol-gel-coated Ti6Al4V. Panel (a) depicts the evolution at 0 s, (b) at 240 s, (c) at 480 s and (d) at 960 s. Peaks A and a, represent elemental Ti; B and b, TiO; C and c, Ti₂O₃; D and d, TiO₂.

mean analyses of two liquid probes: water (polar) and methylene iodide (dispersive). The contact angles and surface energy (dyn/cm) of the substrates are shown in Table 2. Both passivated and sol-gel-coated surfaces exhibited good wettability and relatively high surface energy; however, wettability by water was significantly different for the two substrates ($p = 0.014$), whereas the wettability by methylene iodide was equivalent ($p = 0.417$). A significantly higher polar component of the surface energy was measured on the sol-gel-coated substrate, as compared with the passivated surface ($p < 0.05$), and the latter had a significantly lower dispersive component ($p < 0.05$).

3.3. Morphology and roughness

Visual inspection of the sol-gel-coated substrate indicated a rough surface with a dull grayish brown color, and continuous deposition resulted in increased brown coloration (not shown). Representative SEM topographs of 5-layer sol-gel-coating and passivated substrates are shown in Fig. 6. Striations from the machining process are visible on the passivated substrate surface. The sol-gel-coated substrate showed a coated surface with amorphous titanium oxide precipitates and a range of nanopores (5–50 nm) and micropores. The AFM images of surfaces,

shown in Fig. 7, revealed spherical oxide domains that appeared clustered on the substrate coated with 5 layers of sol-gel, whereas finer and flatter structures were observed on the passivated substrate. The topography of the 5-layer, as well as 15-layer, coated samples are shown in Fig. 8 and the horizontal line below represents the path of the profile. The 15-layer film appeared more uniform and smoother compared to the 5-layer film. The qualitative differences between the sample groups were supported by significant differences in the rms roughness values (5 gel layers = 177.3 ± 52.1 nm, 15 gel layers = 72.3 ± 10.9 nm and passivated = 38.2 ± 1.7 nm).

To evaluate surfaces for potential protein adsorption, AFM images and roughness values were obtained for the samples following a 24-h incubation in serum-containing media (Fig. 9). The rms roughness values for the passivated (23 ± 9) and sol-gel-coated (146 ± 32) substrates after incubation in this media were both lower than the values obtained from naive samples (see paragraph above), consistent with the deposition of serum proteins onto the material surface.

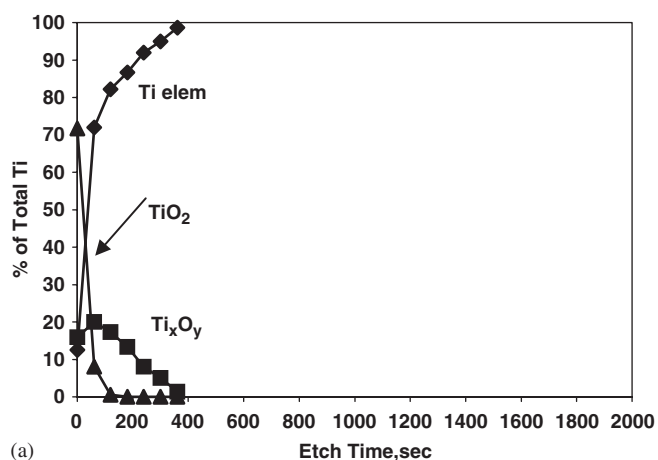
3.4. Cell adhesion and morphology

The results shown in Fig. 10 indicate that a significantly greater number ($p < 0.05$) of MC3T3-E1 osteoprogenitor

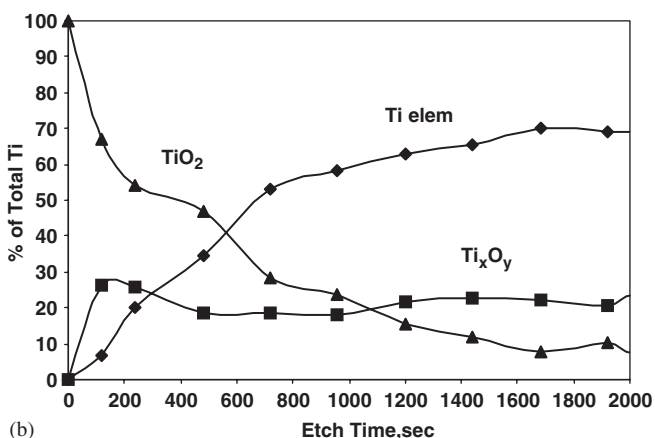
cells adhered to the sol-gel-coated samples, as compared with passivated substrates, at both 1 and 24 h following cell seeding. The morphology of the adherent cells was also evaluated, using a phalloidin staining method to visualize the actin cytoskeleton (Fig. 11). At 1 h after seeding (panels a and b), the cell shape and degree of cell spreading were similar on the two surfaces, although more cells appeared to be bound to the sol-gel-coatings. After 24 h (panels c and d), the actin filaments of cells adherent to the passivated substrates were aligned in parallel with the surface striations. In contrast, the cells on the sol-gel-coated substrates appeared multi-directional, and conformed to the concavities of the surface.

3.5. Mineralization

To evaluate the capacity of sol-gel coatings to support osteoblastic differentiation of MC3T3-E1 cells, cells were seeded onto the substrates, and then grown in differentiation-inducing media for 14 days. Cultures were then incubated with calcein dye in order to label the mineralized nodules (Fig. 12). Fluorescent microscopy of the stained cultures indicated that a substantially greater number of nodules were present on the cell cultures adherent to sol-gel-coated, as compared with passivated surfaces. Similarly, representative SEM micrographs (Fig. 13) showed that the sol-gel surface was covered by an extensive, multilayer coating of nodule-like structures. In



(a)



(b)

Fig. 5. XPS sputter depth profile plots showing the Ti chemical states as a percentage of the total Ti for the passivated and the 5-layer sol-gel-coated Ti6Al4V substrates: (a) passivated, and (b) 5-layer sol-gel-coated Ti6Al4V (\blacktriangle = TiO_2 , \blacklozenge = Ti elem, \blacksquare = Ti_xO_y).

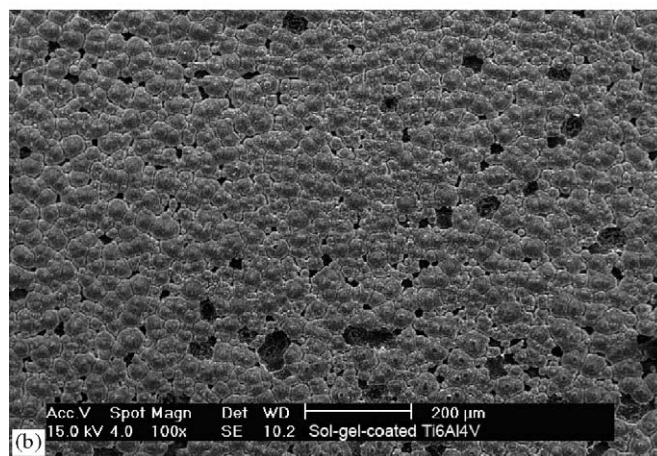
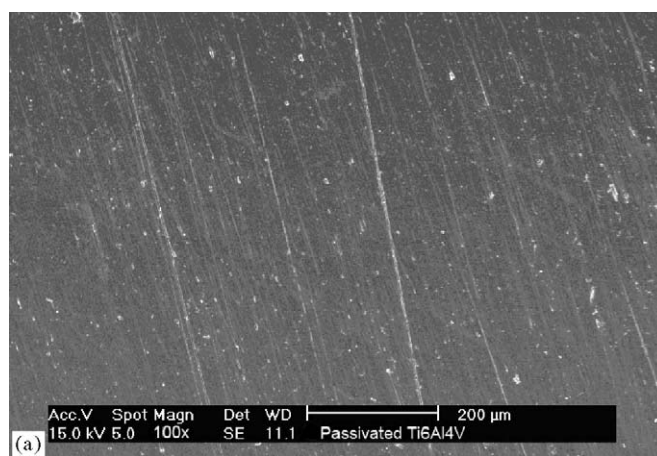


Fig. 6. SEM images showing different topographies after treatment. The horizontal line represents the path of the profile: (a) passivated and (b) 5-layer sol-gel-coated Ti6Al4V ($\times 100$).

Table 2
Contact angle and surface energy

Samples	Water (deg.)	Methylene iodide (deg.)	Dispersive component (dyn/cm)	Polar component (dyn/cm)	Total surface energy (dyn/cm)
Passivated ($n = 18$)	32 ± 4	19 ± 3	35 ± 1	30 ± 3	65 ± 2
Sol-gel coated ($n = 9$)	18 ± 5	18 ± 5	33 ± 1	37 ± 2	70 ± 2

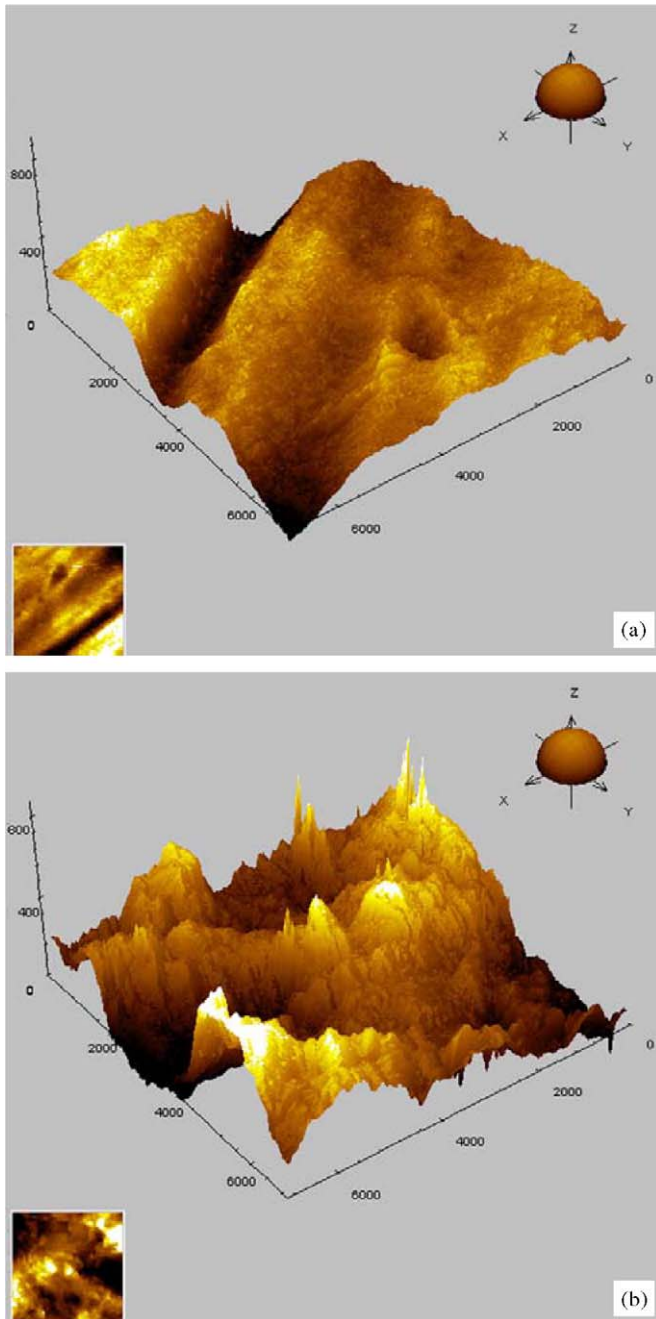


Fig. 7. AFM images showing the microtopography of substrate surface: (a) passivated and (b) 5-layer sol-gel-coated Ti6Al4V substrates ($7\ \mu\text{m} \times 7\ \mu\text{m}$).

contrast, only a few nodular structures were detected on passivated surfaces, and exposed cell bodies were readily apparent. A higher magnification of the nodules on sol-gel surfaces revealed a coral-like appearance (inset), and EDS analysis indicated the presence of elemental Ca (15.92%) and P (15.89%), consistent with the formation of a mineralized matrix.

4. Discussion

Results from the current investigation show that samples prepared by the stepwise sol-gel process have a signifi-

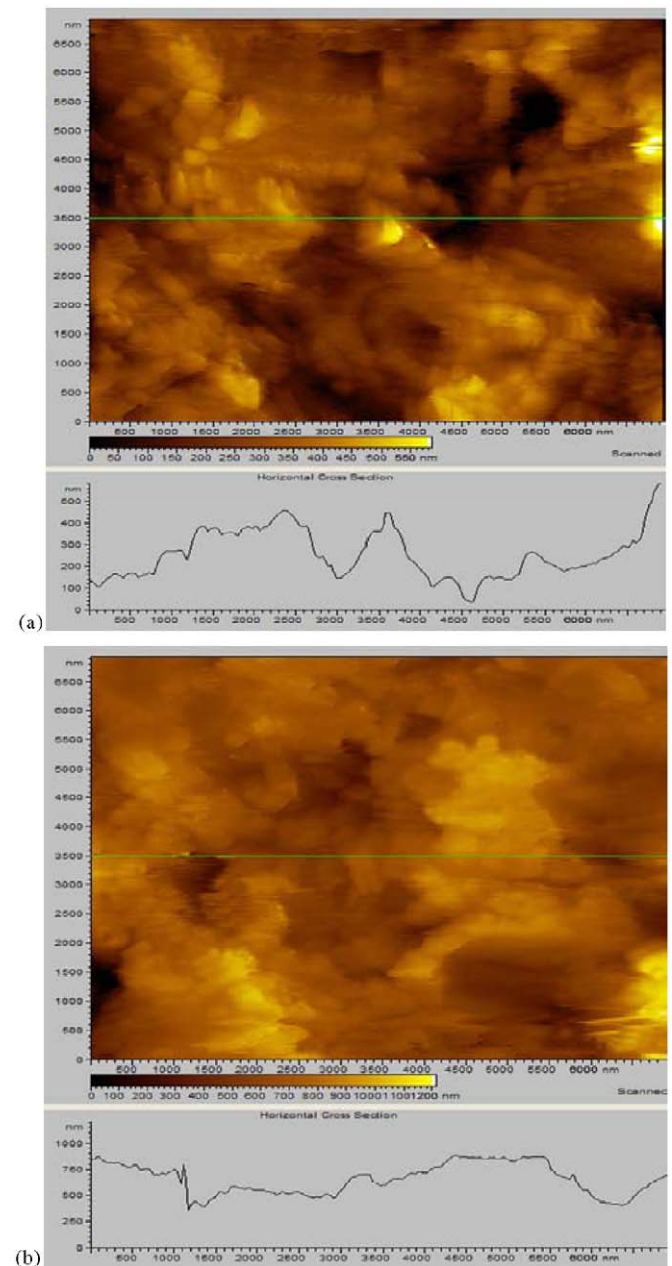


Fig. 8. AFM images showing the microtopography of coated substrates after sol-gel deposition. (a) After coating with 5 layers and (b) 15 layers ($7\ \mu\text{m} \times 7\ \mu\text{m}$).

cantly different oxide roughness, topography, composition, and wettability than standard passivated surfaces, and that these factors influence the behavior of osteoblastic MC3T3-E1 cells. A typical cycle of the sol-gel process involves: (a) the activation of the surface with OH groups; (b) the reaction of the hydroxylated surface with metal alkoxides in solution to form covalently bound surface monolayers of the alkoxide; (c) the removal of excessively adsorbed or physisorbed alkoxide by solvent rinsing; and (d) the hydrolysis of the chemisorbed alkoxide monolayer and the formation of new surface OH groups by immersion in water. Under carefully controlled conditions, a

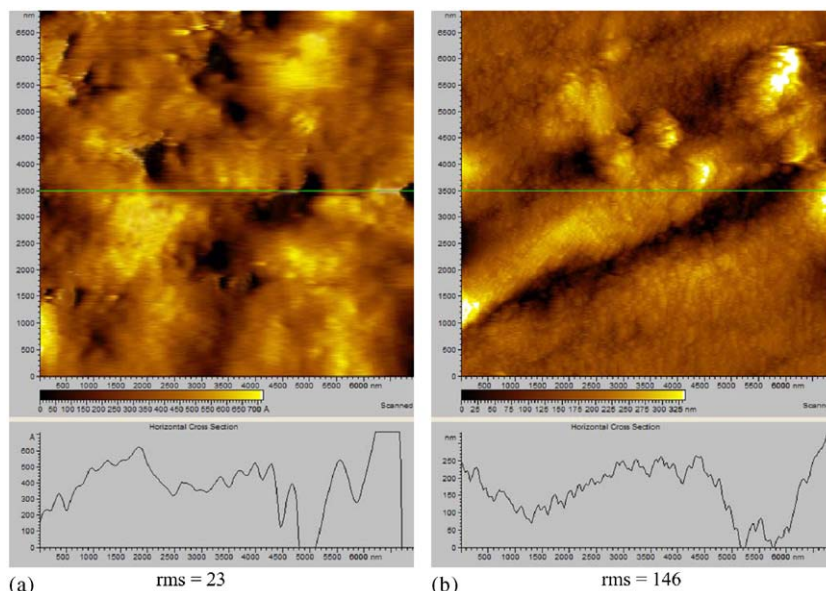


Fig. 9. AFM images showing the microtopography and average root mean square roughness (rms) after the substrates were immersed in serum media ($7\mu\text{m} \times 7\mu\text{m}$): (a) passivated and (b) 5-layer sol-gel-coated Ti6Al4V.

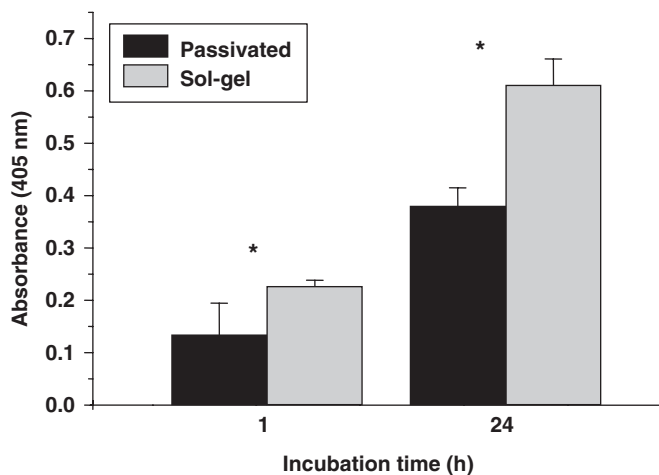


Fig. 10. MC3T3-E1 cell adhesion to passivated and 5-layer sol-gel-coated surfaces, as measured by hexosaminidase assay. Values represent the means and standard errors for three independent experiments, with each experiment performed in triplicate. * indicates statistically significant difference ($p < 0.05$).

nanometer-thick layer of the metal oxide is formed. Each of the sol-gel deposition cycles is independent of the others, and by repeating the process several times, a multilayer structure of the oxide (typically a Ti–O–Ti network) can be produced.

The sol-gel coating imparted higher surface OH functionalities than those produced by HNO_3 passivation (34.6% and 19.5%, respectively, Fig. 3). The abundance of OH groups and predominance of TiO_2 on the surface are consistent with earlier reports on the oxide composition [35,39]. Furthermore, the depth profile analysis suggests that the sol-gel coating is composed of an outer surface

layer of TiO_2 and an inner layer of Ti_2O_3 and TiO suboxide states. The data in Fig. 5 show that prior to sputter etching (at 0 s etch time), the Ti2p lineshape can be described satisfactorily by two peaks assigned to the spin-orbit doublet, $\text{Ti}2p_{3/2}$ (at ~ 459.0 eV, labeled D) and $\text{Ti}2p_{1/2}$ (at ~ 464.8 eV, labeled d), for the TiO_2 chemical state [49]. No evidence for the presence of the substoichiometric Ti_2O_3 and TiO oxides were found for this surface. Upon Ar^+ ion sputtering, lower oxidation states of Ti appear: peaks A and a, at ~ 454.0 and ~ 460 eV, respectively, are assigned to the elemental Ti^0 state; peaks B and b, at ~ 455.5 and ~ 461.4 eV, respectively, are assigned to the TiO state; and peaks C and c, at ~ 457.5 and ~ 463.0 eV, respectively, are assigned to the Ti_2O_3 state. At increasing sputter etch times, the contribution of TiO_2 states decrease while those of the Ti_2O_3 , TiO and elemental Ti^0 states increase. At even longer sputter etch times (for example at 960 s and beyond), the substoichiometric Ti_2O_3 and TiO oxide contributions progressively decrease while that of the elemental Ti^0 state continuously increases. Thus, TiO_2 is progressively and successively reduced to Ti_2O_3 , then to TiO, and finally, to Ti^0 . However, it is also known from previous XPS sputter depth profile studies of TiO_2 and other reducible metal oxides [50] that a significant portion of the observed Ti_2O_3 and TiO suboxide states is not originally present in the analyzed layer but is due to the preferential sputtering of lighter O atoms by Ar^+ ions. An accurate value for the contribution of this Ar^+ ion-induced reduction to the various Ti oxide states originally present in the subsurface region is difficult to determine, and so for this reason, only a substoichiometric “ Ti_xO_y ” state in the depth profile plots in Fig. 5 is reported to represent the combined Ti_2O_3 and TiO components in the oxide film. Nevertheless, the results presented here conform to previous sputter depth profile

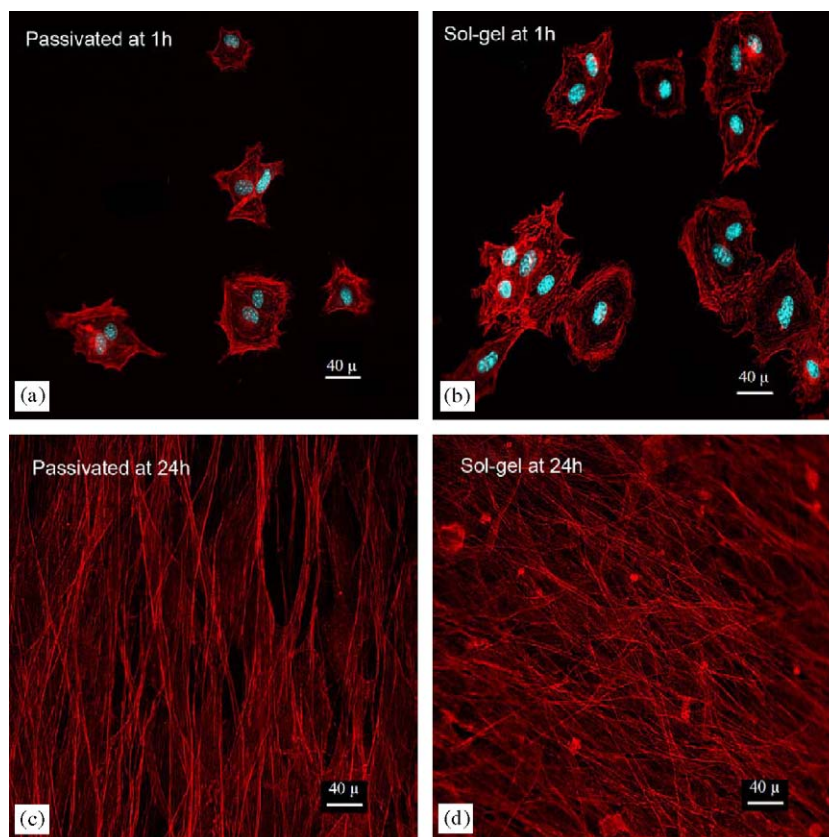


Fig. 11. Phalloidin staining of the actin cytoskeleton after cells adhered on substrates. Panels (a, c) represent MC3T3-E1 cells adherent to passivated Ti6Al4V for 1 or 24 h and panels (b, d) to 5-layer sol-gel-coated Ti6Al4V for 1 or 24 h ($\times 2500$).

studies of TiO₂ films on Ti substrates [50,51 and references therein].

Compositional analysis of the surface also revealed the presence of carbon-dominated contaminants and trace amounts of N, Na, and Cl, due, in part, to the amorphous nature of the non-calcined sol-gel-derived oxide [52]. It is not known whether the presence of these contaminants on the samples affected the wettability behavior of the sol-gel-coated with respect to the passivated substrates. This will be a point of further investigation in the future. The presence of S on the acid-etched surface was attributed to residual H₂SO₄ upon pretreatment and was not expected to affect the oxide formed upon deposition of the alkoxide. It is worth mentioning that the high OH density ($\sim 44.5\%$) or hydroxylation of the substrate surface prior to sol-gel processing was achieved by etching with Piranha acid solution [43].

Although both substrates presented with an oxide composition of TiO₂, the sol-gel-coated substrate had a higher content of OH groups and adsorbed H₂O (Fig. 3) compared to passivated (H₂O not detected) substrate. The higher wettability of the sol-gel-coated surface can be attributed in part to the presence of these OH groups, as evidenced by the lower polar (water) contact angle or higher polar component of the total surface energy. The high polar component values clearly show the predomi-

nance of polar groups on the sol-gel-coated substrates, whereas the lower polar component of the passivated surface may be attributed to the lack of these polar groups. The consequential increase in the interfacial free energy could promote events such protein adsorption and cell adhesion [11,14].

The greater hydrophilicity of the sol-gel coating could potentially affect the amount, type, and/or conformation, of proteins that become adsorbed to the material surface from either the serum within tissue culture media, or body fluids within the in vivo environment. For example, it has been shown that increased hydrophilicity of titanium, caused by roughening of the surface, promoted increased adsorption of fibronectin and vitronectin, but not of albumin, a serum protein that is generally considered to be non-adhesive [16]. Furthermore, preferential attachment and growth of osteoblastic cells, and enhanced matrix mineralization, has been observed on hydrophilic substrates [53]. The type, density, and conformation of adsorbed proteins, as well as cell type-specific differences in membrane properties and integrin receptor expression, are all important factors that influence tissue development on the implant surface [3–6]. In this study, the surface roughness values for sol-gel-coated and passivated substrates were decreased following incubation in serum-containing media, indicating the adsorption of serum

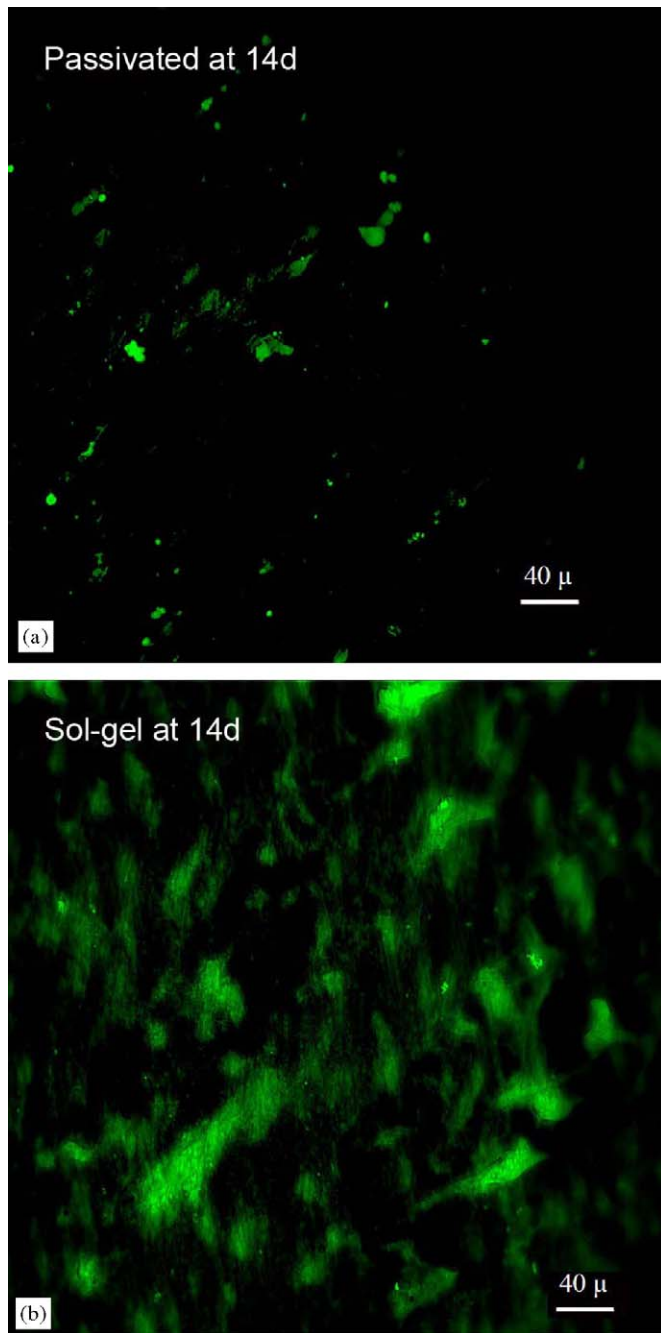


Fig. 12. Calcein labeling of mineralized deposits on substrates at 14 days ($\times 2500$): (a) passivated and (b) 5-layer sol-gel-coated Ti6Al4V.

components. Moreover, the characteristics of the adsorbed serum protein layer, particularly the microtopography and roughness, were clearly different for the sol-gel-coated and passivated surfaces. Further analyses are needed to identify which types of proteins preferentially bind to these substrates.

The adsorption of pro-adhesive blood proteins to the material surface is thought to play a significant role in osseointegration, since these proteins serve as ligands for integrin adhesion receptors. In turn, integrin activation and cell spreading induce the activation of signaling cascades

that ultimately regulate events such as osteoblast differentiation [11]. In the current investigation, it was found that, relative to passivated surfaces, sol-gel coatings stimulated greater MC3T3-E1 cell adhesion, as well as enhanced matrix mineralization, despite the similarity in surface composition of the two substrates. These results are consistent with another study wherein titanium materials with different roughnesses, but only varying in composition by less than 1%, stimulated higher cell adhesion and *in vitro* mineralization [13]. In fact, many studies have suggested that osteoblast attachment is optimal on rougher titanium and titanium alloys [16,18,19], although greater cell adhesion and spreading on smooth Ti alloy has also been reported [12]. It should be noted that the topography of the sol-gel-coated surface was rougher compared to previously reported morphologies of the oxide [39]. The roughness, however, decreased after 15 dipping cycles, which indicates that the topography can be controlled with further deposition. The change in roughness and heterogeneity of the surface can also affect the surface energy of the substrate, and thus, its bioreactivity [14]. Investigation of the effects of increasing the number of oxide layers on the bioreactivity of the coated surface will be the subject of future studies.

It was noted that an extensive coating of a non-stoichiometric apatite-like substance was formed on the sol-gel-coated substrates following cell growth in osteogenic media. It is possible that sol-gel coatings demonstrate an increased capacity to initiate calcium phosphate nucleation, relative to passivated surfaces, leading to the formation of a calcium apatite layer. In general, the oxide that is formed by SSP possesses abundant OH groups (Si-OH or Ti-OH), which could promote electrostatic attraction of calcium ions or hydrogen bonding with phosphate groups. For example, Li et al. [31] suggested that nucleation of calcium phosphate from simulated body fluid was due to OH groups on sol-gel-derived titanium. Furthermore, calcium nucleation on sol-gel-derived titania/hydroxyapatite coatings stimulated osteoblast cell attachment and differentiation [54]. The enhanced cell adhesion and matrix mineralization observed on sol-gel coatings synthesized in the current study are consistent with these prior reports, however further experiments will be required to evaluate whether increased calcium phosphate nucleation plays a role in this process.

5. Conclusion

The modification of Ti alloy by stepwise surface sol-gel processing produced an altered surface topography, composition and wettability which, in turn, promoted increased attachment of osteoblasts and enhanced formation of a mineralized matrix. It is anticipated that the surface activation and bioreactivity of titanium alloys prepared by this novel multilayer deposition process will allow control of the material surface properties at the

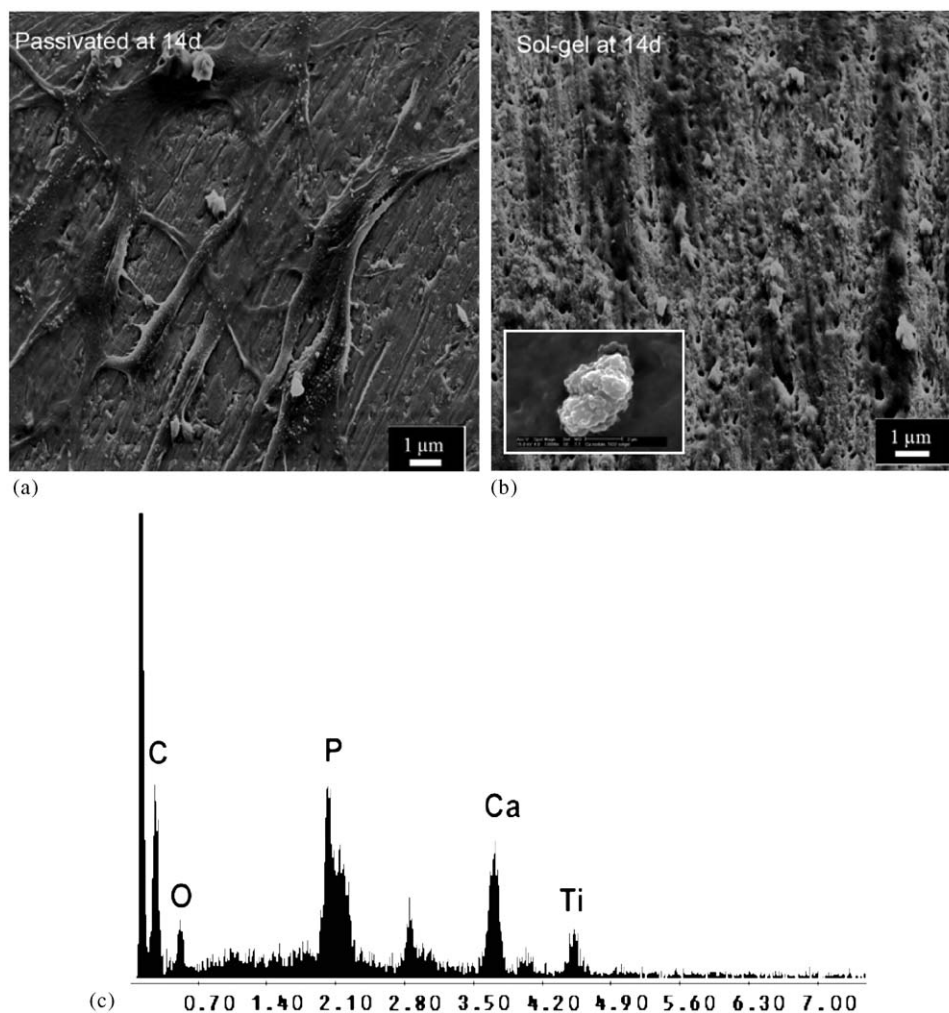


Fig. 13. SEM micrographs of the mineralized substrates: (a) passivated, (b) sol-gel-coated Ti6Al4V (inset represents higher magnification of a nodular structure), and (c) EDS profile of the nodular structure shown in the inset for panel b.

nanometer level, producing coatings with more relevant physico-chemical and biological properties.

Acknowledgements

This work was supported, in part, by grants from NSF (NSF-DMR-0315565), and the Whitaker Foundation. Dr. M.C. Advincula received stipend support from Bicon, Inc., Boston, MA. The authors wish to thank Dr. Charles Prince, Nutrition Sciences, (UAB) for providing the cells, and also the staff of the Department of Chemistry (UAB) for the use of the AFM and contact angle meter.

References

- [1] Horbett TA. Biological activity of adsorbed proteins. In: Malmsten M, editor. *Biopolymers at interfaces, Surfactant science series 75*. New York, NY: Marcel Dekker; 1998. p. 393.
- [2] Anderson JM, Gristine AG, Hanson SR. Host reactions to biomaterials and their evaluation. In: Ratner BD, Hoffman AS, Schoen FJ, Lemons JE, editors. *Biomaterials science; an introduction to materials in medicine*, vol. 1. San Diego, CA: Academic Press; 1996. p. 165–214.
- [3] Siebers MC, ter Brugge PJ, Walboomers XF, Jansen JA. Integrins as linker proteins between osteoblasts and bone replacing material. A critical review. *Biomaterials* 2005;26:137–46.
- [4] Puleo DA, Nanci A. Understanding and controlling the bone-implant interface. *Biomaterials* 1999;20:2311–21.
- [5] Lebaron R, Athanasiou K. Extracellular matrix cell adhesion peptides: functional applications in orthopedic materials. *Tissue Eng* 2000;6:85–103.
- [6] Anselme K. Osteoblast adhesion on biomaterials. *Biomaterials* 2000;21:667–81.
- [7] Hlady V, Buijs J. Protein adsorption on solid surfaces. *Curr Opin Biotech* 1996;7:72–7.
- [8] Gray JJ. The interaction of proteins with solid surfaces. *Curr Opin Struct Biol* 2004;14:110–5.
- [9] Kasemo B, Lausmaa J. Biomaterial and implant surface: a surface science approach. *Int J Oral Maxillofac Implants* 1988;3:83–101.
- [10] Albrektsson T, Branemark PI, Hansson HA, Kasemo B, Larson K, Lundstrom I, et al. The interface zone of inorganic implants in vivo: titanium implants in bone. *Ann Biomed Eng* 1983;11:1–27.
- [11] Boyan BD, Hummert TW, Dean DD, Schwartz Z. Role of material surfaces in regulating bone and cartilage cell response. *Biomaterials* 1996;17:137–46.
- [12] Anselme K, Linez P, Bigerelle M, Le Maguer D, Le Maguer A, Hardouin P, et al. The relative influence of the topography and chemistry of Ti6Al4V surfaces on osteoblastic cell behavior. *Biomaterials* 2000;21:1567–77.

- [13] Ahmad M, Gawronski D, Blum J, Goldberg J, Gronowicz G. Differential response of human osteoblast-like cells to commercially pure (cp) titanium grades 1 and 4. *J Biomed Mater Res* 1999;46:121–31.
- [14] Baier RE, Meyer AE, Natiella JR, Natiella RR, Carter JM. Surface properties determine bio-adhesive outcomes: methods and results. *J Biomed Mater Res* 1984;18:337–55.
- [15] Webb K, Hlady V, Tresco P. Relationships among cell attachment, spreading, cytoskeletal organization and migration rate for anchorage dependent cells on model surfaces. *J Biomed Mater Res* 2000;49:362–8.
- [16] Deligianni DD, Katsala N, Ladas S, Sotiropoulou D, Amedee J, Missirlis YF. Effect of surface roughness of the titanium alloy Ti6Al4V on human bone marrow cell response and on protein adsorption. *Biomaterial* 2001;22:1241–51.
- [17] Healy KE, Thomas CH, Rezanian A, Kim JE, McKeown PJ, Lom B, et al. Kinetics of bone cell organization and mineralization on materials with patterned surface chemistry. *Biomaterials* 1996;17:195–208.
- [18] Bowers KT, Keller JC, Randolph BA, Wick DG, Michaels CM. Optimization of surface micromorphology for enhanced osteoblast responses in vitro. *Int J Oral Maxillofac Implants* 1992;7:302–10.
- [19] Groessner-Schreiber B, Tuan RS. Enhanced extracellular matrix production and mineralization by osteoblasts cultured on titanium surfaces in vitro. *J Cell Sci* 1992;101:209–17.
- [20] Larsson C, Thomsen P, Lausmaa J, Rodahl M, Kasemo B, Ericson LE. Bone response to surface modified titanium implants: studies on electropolished implants with different oxide thicknesses and morphology. *Biomaterials* 1994;15:1062–74.
- [21] Kumagai H, Matsumoto M, Toyoda K, Obara M, Suzuki M. Fabrication of titanium oxide thin films by controlled growth with sequential surface chemical reactions. *Thin Solid Films* 1995;263:47–53.
- [22] Wuhrer R, Yeung WY, Phillips MR, McCredie G. Study on d.c. magnetron sputter deposition of titanium aluminum nitride thin films: effects of aluminum content on coating. *Thin Solid Films* 1996;290–291:339–42.
- [23] Kozuka H, Zhao G, Yoko T. Sol-gel preparation and photoelectrochemical properties of TiO₂ films containing Au and Ag metal particles. *Thin Solid Films* 1996;277:147–54.
- [24] Kilpadi DV, Raikar GN, Liu J, Lemons JE, Vohra Y, Gregory JC. Effect of surface treatment on unalloyed titanium implants: spectroscopic analyses. *J Biomed Mater Res* 1998;40:646–59.
- [25] Pan J, Liao H, Leygraf C, Thierry D, Li J. Variation of oxide films on titanium induced by osteoblast like cell culture and influence of an H₂O₂ pretreatment. *J Biomed Mater Res* 1998;40:244–56.
- [26] Diniz MG, Soares GA, Coelho MJ, Fernandes MH. Surface topography modulates the osteogenesis in human bone marrow cell cultures grown on titanium samples prepared by a combination of mechanical and acid treatments. *J Mater Sci Mater Med* 2002;13:421–32.
- [27] Wen HB, de Wijn JR, Cui FZ, de Groot K. Preparation of calcium phosphate coatings on titanium implant materials by simple chemistry. *J Biomed Mater Res* 1998;41:227–36.
- [28] Lev O, Wu Z, Bharathi S, Glezer V, Modestov A, Gun J, et al. Sol-gel materials in electrochemistry. *Chem Mater* 1997;9:2354–75.
- [29] Jokinen M, Päätsi M, Rahiala H, Peltola T, Ritala M, Rosenholm JB. Influence of sol and surface properties on in vitro bioactivity of sol-gel derived TiO₂ and TiO₂-SiO₂ films deposited by dip-coating method. *J Biomed Mater Res* 1998;42:295–302.
- [30] Haddow DB, Kothari S, James PF, Short RD, Hatton PV, van Noort R. Synthetic implant surfaces 1: The formation and characterization of sol-gel titania films. *Biomaterials* 1996;17:501–7.
- [31] Li P, Ohtsuki C, Kokubo T, Nakanishi K, Soga N, de Groot K. The role of hydrated silica, titania and alumina in inducing apatite on implants. *Biomaterials* 1994;28:7–15.
- [32] Li P, de Groot K. Calcium phosphate formation within sol-gel prepared titania in vitro and in vivo. *J Biomed Mater Res* 1993;27:1495–500.
- [33] Areva S, Peltola T, Sailyoja E, Laajalehto K, Linden M, Rosenholm JB. Effect of albumin and fibrinogen on calcium phosphate formation on sol-gel derived titania coatings in vitro. *Chem Mater* 2002;14:1614–21.
- [34] Dieudonne SC, van den Dolder J, Ruijter JE, Paldan H, Peltola T, van't Hof M, et al. Osteoblast differentiation of bone marrow stromal cells cultured on silica gel and sol-gel derived titania. *Biomaterials* 2002;23:3041–51.
- [35] Ichinose I, Senzu H, Kunitake T. Stepwise adsorption of metal alkoxides on hydrolyzed surfaces: a surface sol-gel process. *Chem Lett* 1996;1:831–2.
- [36] He J, Ichinose I, Fujikawa S, Kunitake T, Nakao A. A general efficient method of incorporation of metal ions into ultrathin TiO₂ films. *Chem Mater* 2002;14:3493–500.
- [37] Acharya K, Kunitake T. A general method for fabrication of biocompatible surfaces by modification with titania layer. *Langmuir* 2003;19:2260–6.
- [38] Kunitake T, Lee S. Molecular imprinting in ultrathin titania gel films via surface sol-gel process. *Anal Chem Acta* 2004;504:1–6.
- [39] Kimizuka N, Tanaka M, Kunitake T. Spatially controlled synthesis of protein/inorganic nano-assembly: alternate molecular layers of Cyt c and TiO₂ nanoparticles. *Chem Lett* 1999;1:1333–4.
- [40] Ito T, Okayama Y, Shiratori S. The fabrication of organic/inorganic multilayer by wet process and sequential adsorption method. *Thin Solid Films* 2001;393:138–42.
- [41] Fang M, Kim CH, Martin BR, Mallouk TE. Surface sol-gel synthesis of ultrathin titanium and tantalum oxide films. *J Nanoparticle Res* 1999;1:43–9.
- [42] Hashizume M, Kunitake T. Preparation and functionalization of self-supporting (polymer/metal oxide) composite ultrathin films. Focus on Nanotechnology in RIKEN II. *RIKEN Rev* 2001;38:36–9.
- [43] Nanci A, Wuest JD, Peru L, Brunet P, Sharma V, Zalzal S, et al. Chemical modification of titanium surfaces for covalent attachment of biological molecules. *J Biomed Mater Res* 1998;40:324–35.
- [44] Seah MP. Quantification of AES and XPS. In: Briggs D, Seah MP, editors. *Practical surface analysis*, vol. 1. New York, NY: Wiley; 1990. p. 207.
- [45] Goldstein JI, et al. *Scanning electron microscopy and X-ray microanalysis*. 3rd ed. New York: Kluwer Academic/Plenum Publishers; 2003. p. 286–288.
- [46] Landegren U. Measurement of cell numbers by means of endogenous enzyme hexosaminidase. Applications to detection of lymphokines and cell surface antigens. *J Immunol Methods* 1984;67:379–88.
- [47] Hale LV, Ma YF, Santerre RF. Semi-quantitative fluorescence analysis of calcein binding as a measurement of in vitro mineralization. *Calcif Tissue Int* 2000;67:80–4.
- [48] McCafferty E, Wightman JP. Determination of the concentration of surface hydroxyl groups on metal oxide films by a quantitative XPS method. *Surf Int Anal* 1998;26:549–64.
- [49] Moulder JF, Stickle WF, Sobol PE, Bombardier KD. *Handbook of X-ray photoelectron spectroscopy*, Physical electronics division. Eden-Prairie, MN: Perkin-Elmer Corporation; 1980.
- [50] Hofman S. Depth Profiling in AES and XPS. In: Briggs D, Seah MP, editors. *Practical surface analysis*, vol. 1. New York, NY: Wiley; 1990. p. 169–72.
- [51] McCafferty E, Wightman JP. An X-ray photoelectron spectroscopy sputter profile study of the native air-formed oxide film on titanium. *Appl Surf Sci* 1999;143:92–100 also the references therein.
- [52] Esposito M, Lausmaa J, Hirsch JM, Thomsen P. Surface analysis of failed oral titanium implants. *J Biomed Mater Res* 1999;48:559–68.
- [53] Liao H, Andersson AS, Sutherland D, Petronis S, Kasemo B, Thomsen P. Response of rat osteoblast-like cells to microstructured model surfaces in vitro. *Biomaterials* 2003;24:649–54.
- [54] Ramires PA, Romito A, Cosentino F, Milella E. The influence of titania/hydroxyapatite composite coatings on in vitro osteoblast behaviour. *Biomaterials* 2001;22:1467–74.